A Fourier-based Semi-Analytical Model for Foil-Wound Solid-State-Transformers

A Fourier-based Semi-Analytical Model for Foil-Wound Solid-State-Transformers

Siamak Pourkeivannour[1], Mitrofan Curti[1], Coen Custers[1], Andrea Cremasco[1], Uwe Drofenik[2], and Elena A. Lomonova [1]
[1]Department of Electrical Engineering, Eindhoven University of Technology, 5612 AZ Eindhoven, The Netherlands
[2]ABB Research Center Switzerland, Department of Power Electronics, 5405 Baden, Switzerland

A mesh-free semi-analytical Fourier-based method is presented to evaluate the frequency-dependent losses in the windings of SSTs with foil-wound transformers. In the employed diffusion equation, which accounts for induced eddy currents, the imposed current density and conductivity in the transformer window area are represented using spatial Fourier series and method of images. As a result, induced current density distribution in foil conductors and AC loss in MFTs is calculated using the semi-analytical method. The proposed method is verified using Finite Element Method (FEM). It is observed that with the considered approach one can estimates the AC winding loss in the frequency range of 5-25 kHz, with 2.7% maximum absolute error and approximately 2.5 times less number of degrees-of-freedom compared to FEM computations.

***Index Terms*—Solid State transformers, medium frequency transformers, foil winding, eddy current, Fourier based analysis, analytical modeling of electromagnetic fields.**

I. Introduction

SOLID STATE TRANSFORMERS (SSTs) are power conversion systems composed of two power electronic stages coupled to the primary and secondary sides of a medium frequency transformer (MFT). While the power electronics enable improved control of the terminal voltages and currents as well as the reactive and active power flows, MFT provides reduced volume and weight in the isolation stage. These benefits makes SSTs an emerging alternative to low frequency transformers for renewable energy resources, smart grids and traction systems. However, these improvements introduce new challenges in the design of novel SSTs [1]. The considerations toward heat management of the increased power density, as well as the medium voltage (MV) isolation requirements for reduced geometric dimensions of MFTs becomes important. Therefore, the accurate modeling of MFTs in the design approaches is a necessity.

The previous research direction in developing high power, efficient MFT designs were mostly based on the utilization of litz wire. Multiple single insulated strands in the litz wire limit the frequency-dependent skin effect loss. Subsequently, employing twisted and interleaved winding topologies with litz wire brings reduction of proximity effect loss in MFTs [2]. However, the manufacturing challenges of ultra-thin strand conductors and the low fill factor of litz wire have promoted foil conductors for MFT windings [3]. Foil-wound MFTs exhibit high utilization of window area as well as reduced manufacturing cost. However, twisting and interleaving ultra-thin and high foil conductors is not practical. Thus, the frequency-related winding loss becomes a dominating component in analyzing the general system operation performance of foil-wound SSTs.

This study aims to facilitate the AC losses computation by developing a semi-analytical approach. The proposed method is a mesh-free Fourier-based method, in which the model parameters are described by periodic functions to analyze electromagnetic field distributions [4]. The proposed method is implemented on a foil-wound SST to find a 2D expression for the induced current density distribution inside the conducting regions in the MFT window area.

This paper is structured as follows: Section I is a brief survey on the classical methods for calculating AC losses in MFTs. Section II details the proposed semi-analytical method. Finally, Section III compares the accuracy and the computational cost of the proposed method with FEM.

II. Classical Methods

The predictions of the current density distribution and the AC losses due to skin and proximity effects have been addressed in several studies mentioned in [5]. The most referred method is the "ready-to-use" Dowell's 1D expression for AC resistance of transformer windings [6]. This method assumes the height of the foil windings equal to the height of the winding window, which enables a uni-directional magnetic field and current density distribution in the window area of MFTs. However, due to the insulation requirements in higher voltage applications, the height of the winding is limited within the isolation distances in the window area of the transformer. This constraint introduces some deviations from Dowell's method. The magnetic field gets a second-dimensional component causing high current density concentrations in the foil corners, called the "edge effect" [7]. The error in Dowell's equation relative to a full cylindrical solution can be as much as nearly 33% [8]. However, the deviation of classical methods is intensely higher in MFTs, since the isolation clearance distance between core and windings increases.

Later, Bennett [9] and Ferreira [10], [11] modified the Dowell's method by introducing porosity factor (η) into closed-

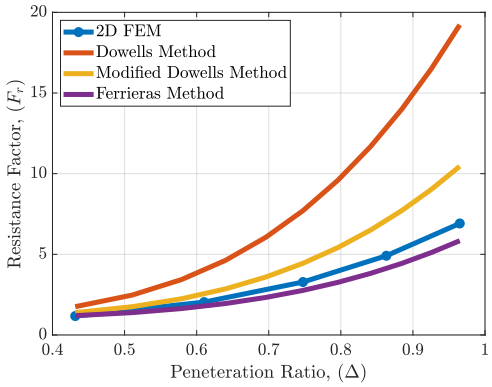

Fig. 1. The comparison of calculated resistance factor using classical methods and 2D FE method for an arbitrary reference MFT model with $\eta = 0.72$.

form equation of Dowell. Porosity factor is the geometric ratio of the conductor height to window height of MFT. However, accurate estimation of the 2D current distribution in high-frequency applications is mostly achieved using FEM analysis [12]. Fig. 1 shows the deviation of classical methods in calculating resistance factor compared to FEM for an arbitrary foil-wound MFT. Resistance factor F_r is the ratio of AC to DC resistances, and penetration ratio Δ, is defined as:

$$\Delta = \frac{d_w}{\sqrt{\frac{1}{\pi \mu \sigma f}}}, \tag{1}$$

where d_w is the conductor thickness, μ, σ and f are the permeability, conductivity of the conductor and frequency, respectively.

The accuracy of FEM comes with the cost of extra fine mesh, implying high computational cost, making it a less-preferable choice for design tools. In addition to research contributed to 2D eddy loss estimations by introducing porosity correction coefficients, utilization of empirical approaches is proposed in [5]. However, these methods are mainly valid for specific geometries and need Preprocessing. Thus, the need for a flexible and easy-to-apply method is a research question not answered yet.

III. Semi-Analytical Fourier-Based Method

The concept of the proposed 2D semi-analytical method is illustrated in Fig. 2. To solve the 2D induced current density distribution in the foils of the winding, conducting and non-conducting surfaces in the window area are divided into multiple regions. By using method of images, it is assumed that the window area is periodic in axial direction. The imposed current density and conductivity of the conducting regions are represented using spatial harmonic coefficients of a Fourier series. Since the relative permeability in the ferromagnetic core materials is excessively higher than the permeability in the conducting and non-conducting materials, it assumed that the core has an infinite permeability. This assumption enables replacing the core domain by Neuman boundary conditions (BC) on the window area boundaries.

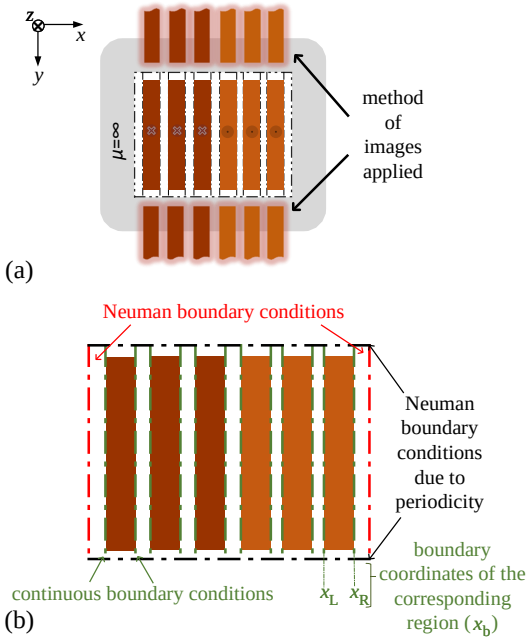

Fig. 2. The geometric model of the window area of a MFT and the implementation of the proposed method. (a) Method of images applied to the window area of MFT. (b) Conducting and non-conducting regions and the boundary conditions.

A. Magnetic Field Formulation

The 2D electromagnetic field distribution in the window area is solved using z-axis magnetic vector potential, $A_z(x, y)$. Based on the derivative form of Maxwell's equations and the constitutive relations, Laplace equation for non-conducting regions and Poisson equation for conducting regions can be derived as:

$$\nabla^2 A_z(x, y) = 0, \tag{2}$$

$$\nabla^2 A_z(x, y) = -\mu \; J_z(x, y), \tag{3}$$

where $J_z(x, y)$ is the 2D current density distribution in the conducting regions. The current density is composed of two terms; the imposed and the induced current densities. Where the induced current density is defined by:

$$J_z^{\text{ind}}(x, y) = -\sigma(y) \; \frac{\partial A_z(x, y)}{\partial t}, \tag{4}$$

the diffusion equation for conducting regions is derived as:

$$\frac{\partial^2 A_z(x, y)}{\partial x^2} + \frac{\partial^2 A_z(x, y)}{\partial y^2} = -\mu \left[J_z^{\text{imp}}(y) - \text{j}\omega\sigma(y) A_z(x, y) \right], \tag{5}$$

where ω is the angular frequency of the imposed current.

B. Fourier-based Semi-analytical Method

To solve (5), method of images is applied in axial direction of the geometry as shown in Fig. 2. The Fourier series representation of imposed current density and conductivity of foils are expressed as:

$$J_z^{\text{imp}}(y) = \sum_{n=-N}^{N} J_n \; e^{\text{j}k_n y}, \tag{6}$$

$$\sigma(y) = \sum_{n=-N}^{N} \sigma_n \; e^{\mathrm{j}k_n y}. \tag{7}$$

With a half period of the region τ_y, the spatial frequency k_n is defined as:

$$k_n = (n\pi/\tau_y). \tag{8}$$

Since the imposed current density and conductivity, as source terms of the diffusion equation, are expressed using Fourier series, the solution for the magnetic vector potential is in terms of Fourier series as well. After the derivations detailed in [13], the expression for magnetic vector potential expressions in non-conducting regions, $A_z^{\mathrm{non-cond}}$, and conducting regions, A_z^{cond}, are derived as:

$$A_z^{\mathrm{non-cond}} = [\boldsymbol{e}(x - x_{\mathrm{R}})\boldsymbol{a} + \boldsymbol{e}(x_{\mathrm{L}} - x)\boldsymbol{b}] \; e^{\mathrm{j}\boldsymbol{K}y}, \tag{9}$$

$$A_z^{\mathrm{cond}} = \boldsymbol{Q}\left[\boldsymbol{E}(x - x_{\mathrm{R}})\boldsymbol{a} + \boldsymbol{E}(x_{\mathrm{L}} - x)\boldsymbol{b} + \boldsymbol{P}\right] \; e^{\mathrm{j}\boldsymbol{K}y}, \tag{10}$$

where $\boldsymbol{P}$ is the source term of diffusion equation and is expressed by:

$$\boldsymbol{P} = \begin{cases} (\boldsymbol{K}^2 + \mathrm{j}\omega\mu\bar{\boldsymbol{\Psi}})^{-1} \; \mu \; J_n^{\mathrm{imp}}, & \text{for : } \; n \neq 0 \\ -\; \frac{1}{2}\mu \; J_n^{\mathrm{imp}} \; (x - x_{\mathrm{L}})^2, & \text{for : } \; n = 0. \end{cases} \tag{11}$$

Where $\boldsymbol{e}(x)$ and $\boldsymbol{E}(x)$ are diagonal matrices containing $e^{k_n x}$ and $e^{\lambda_n x}$ elements, respectively, $\bar{\boldsymbol{\Psi}}$ is a Toeplitz matrix containing Fourier coefficients of the position dependant conductivity, σ_n.

The multiplication of conductivity and magnetic vector potential in (4), both represented using Fourier series, results in multiplication of two matrices. Matrix $\boldsymbol{Q}$ and $\boldsymbol{\Lambda}$ contain eigenvalues and eigenvectors resulting from the decomposition of the resultant matrix:

$$\boldsymbol{Q}\boldsymbol{\Lambda}^2\boldsymbol{Q}^{-1} = \boldsymbol{K}^2 + \mathrm{j}\omega\mu\bar{\boldsymbol{\Psi}}. \tag{12}$$

The derived equations for the magnetic vector potential are composed of a set of linear equations corresponding to each spatial harmonic. Therefore, a system of linear equations containing the unknowns a_n and b_n for each region can be formed and solved using a set of boundary conditions.

The high aspect ration of the conductor geometry causes the system of equations to be ill-conditioned. To improve the condition number, scaling has been implemented on the coefficients presented in $\boldsymbol{a}$ and $\boldsymbol{b}$, as detailed in [14]. This implementation scales the increasing values of coefficients in $\boldsymbol{a}$ and the reducing values of coefficients in $\boldsymbol{b}$ with respect to the harmonic order of each coefficient. The scaling has been implemented by assigning x_{R} and x_{L} to the formulation as the right and left boundaries of each region.

Next, the expression for the induced current density in conducting regions is achieved by substituting (7) and (10) in (4),

$$J_z^{\mathrm{ind}}(x, y) = (-\mathrm{j}\omega\bar{\boldsymbol{\Psi}})\left[\boldsymbol{Q} \; (\boldsymbol{E}(x - x_{\mathrm{R}}) \; \boldsymbol{a} + \boldsymbol{E}(x_{\mathrm{L}} - x) \; \boldsymbol{b})\right] \; e^{\mathrm{j}\boldsymbol{K}y}. \tag{13}$$

Finally, the loss in the conductors is calculated using the surface integral of the current density in the conducting regions.

$$P_{\mathrm{loss}} = \mathrm{Re}\left\{\frac{1}{2\sigma}\int_S J_z(x, y) \cdot J_z^*(x, y)\mathrm{d}s\right\}. \tag{14}$$

C. Boundary Conditions

The solution for the induced current density distribution in (13) is achieved by applying a set of boundary conditions (BCs) to the boundaries of the regions of the geometry shown in Fig. 2.

Expressions for boundary values of the tangential magnetic field intensity (H_y) and normal flux density (B_x) on the boundaries of conducting regions x_{b} is derived as:

$$H_y = -\frac{1}{\mu}\boldsymbol{Q}\boldsymbol{\Lambda}\left[\boldsymbol{E}(x_{\mathrm{b}} - x_{\mathrm{R}})\boldsymbol{a} - \boldsymbol{E}(x_{\mathrm{L}} - x_{\mathrm{b}})\boldsymbol{b} + B_y^0\right], \tag{15}$$

$$B_x = \mathrm{j}\boldsymbol{K}\boldsymbol{Q}\left[\boldsymbol{E}(x_{\mathrm{b}} - x_{\mathrm{R}})\boldsymbol{a} + \boldsymbol{E}(x_{\mathrm{L}} - x_{\mathrm{b}})\boldsymbol{b} + B_x^0\right]. \tag{16}$$

B_y^0 and B_x^0 are the offset values of the tangential and normal flux densities for each region, expressed by:

$$B_y^0 = m\mu J_0^{\mathrm{imp}} d_{\mathrm{w}}, \tag{17}$$

and

$$B_x^0 = \begin{cases} (\boldsymbol{K}^2 + \mathrm{j}\omega\mu\bar{\boldsymbol{\Psi}})^{-1} \; \mu J_n^{\mathrm{imp}}, & \text{for : } \; n \neq 0 \\ -\; \frac{1}{2}m\mu J_n^{\mathrm{imp}} d_{\mathrm{w}}^2, & \text{for : } \; n = 0, \end{cases} \tag{18}$$

where J_0 is the zero harmonic component of the imposed current density, and m is the turn number of the conducting regions in the winding window.

Similarly, H_y and B_x on the boundaries of non-conducting regions are expressed by:

$$H_y = -\frac{1}{\mu}\boldsymbol{K}\left[\boldsymbol{e}(x_{\mathrm{b}} - x_{\mathrm{R}})\boldsymbol{a} - \boldsymbol{e}(x_{\mathrm{L}} - x_{\mathrm{b}})\boldsymbol{b} + B_y^0\right], \tag{19}$$

$$B_x = \mathrm{j}\boldsymbol{K}\left[\boldsymbol{e}(x_{\mathrm{b}} - x_{\mathrm{R}})\boldsymbol{a} + \boldsymbol{e}(x_{\mathrm{L}} - x_{\mathrm{b}})\boldsymbol{b} + B_x^0\right]. \tag{20}$$

While the core is assumed to be infinitely permeable, the magnetic flux density on the region boundaries adjacent to the core is zero along the tangential axis. By applying the method of images, as shown in Fig. 2 (a), the imposed current density expressed by Fourier series is evenly periodic in the axial direction. This periodicity forces the tangential magnetic field to zero on the upper and lower boundaries of the window area. On the left and right boundaries of the window area, the tangential magnetic field is forced to zero using (19). Consequently, the continuity BCs are applied to the boundaries of the non-conducting and conducting regions, shown in Fig.2 (b). These BCs force continuation of normal magnetic flux density B_x and tangential magnetic field intensity H_y inside the window area.

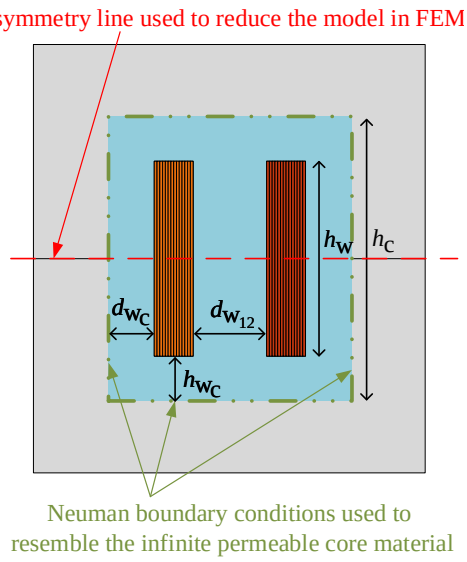

Fig. 3. The geometric model of the window area of the benchmark MFT.

IV. Results and Discussion

To evaluate the accuracy of the proposed method, a shell type MFT benchmark, shown in Fig. 3, is simulated using the semi-analytical method and FEM. Planar symmetry of the model is used to reduce the computations. The geometric specifications of the benchmark are given in Table I. The windings have a conductivity of 37.74 MS/m. To investigate the frequency-dependent performance of the proposed method, the operating frequency is changed from 5 kHz to 25 kHz. The imposed current in foils is equal to 10 A. Initially, the problem is solved using Comsol Multiphysics 5.6 FEM software. The model is meshed using second-order quadratic-shaped elements in the conducting regions and triangular elements in the non-conducting regions of the window area. The maximum size of the mesh elements is limited based on the skin depth of the conductor operating at 20 kHz. In order to determine the required number of the mesh elements in the conducting regions of the model, a mesh convergence study is carried for FEM.

The current density distribution for the first turn of the primary winding, solved using the semi-analytical method, and the the local discrepancy between the semi-analytical method and FEM is shown in Fig. 4. The point-to-point evaluation of the current density shows that the proposed semi-analytic method is in line with FEM results. The highest discrepancy is present at the upper and lower edges of the foil, where the Gibbs effect is present. The problem can be solved by introducing Lancsoz sigma factor to the Fourier coefficients [15]. However, this deviation on the edges has low impact on the cumulative winding loss estimations of the MFT, as seen in Fig. 5.

A comparison of calculated resistance factor of the windings using the semi-analytical and FEM methods is given in Fig. 5. The simulations are done for a frequency range of 5 kHz to 25 kHz. The semi-analytic solution with N=200 gives maximum absolute error, ε, of 2.7% compared to FEM at the frequency of 20 kHz. ε is the maximum

TABLE I
Specifications of the benchmark.

Dimensions	Symbol	Value
Number of winding turns	N_1/N_2	14/14
Foil thickness	d_w	0.5 mm
Foil height	h_w	90 mm
Inter layer insulation thickness	d_{ins}	0.2 mm
Core window height	h_c	126 mm
Winding-core limb clearance distance	d_{wc}	14 mm
Winding-core yoke clearance distance	h_{wc}	30 mm
Inter-winding clearance distance	d_{w12}	36 mm

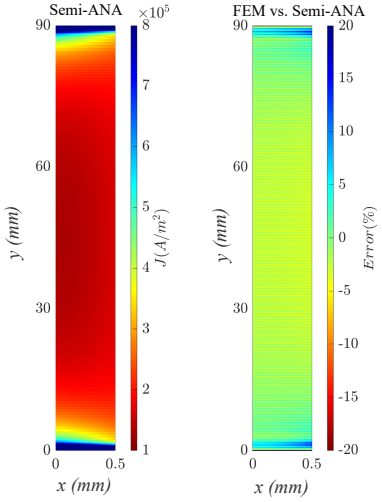

Fig. 4. The current density distribution in one foil calculated by FEM and the semi-analytical method (Semi-ANA) and the local discrepancy distribution between semi-analytic method and FEM ($f = 20$ kHz).

absolute deviation of results in the applied frequency range, calculated with semi-analytical method compared to FEM.

To evaluate the computational cost of the proposed method, the number of degrees-of-freedom (dof) of the semi-analytical method is compared with FEM. As detailed in Table II, for all solutions in the semi-analytical method, number of dof is lower compared to FEM. For the semi-analytical method with N=200 dof is approximately 2.5 times smaller than dof in FEM. In addition to dof, the sparsity of the developed system of linear equations is evaluated for both methods. Either of the two methods shows a high degree of sparsity. To make a fair comparison in terms of computational costs, the developed

TABLE II
A comparison of computational cost and error in semi-analytical method (Semi-ANA) with different harmonic numbers compared to FEM.

Method	dof	Sparsity(%)	Time(s)	ε(%)
FEM	27964	99	12.2	-
Semi-ANA, N=200	11658	96	15.01	2.7
Semi-ANA, N=150	8758	96	5.9	4.3
Semi-ANA, N=120	7018	96	1.54	7.4
Semi-ANA, N=80	4698	96	0.6	10.2

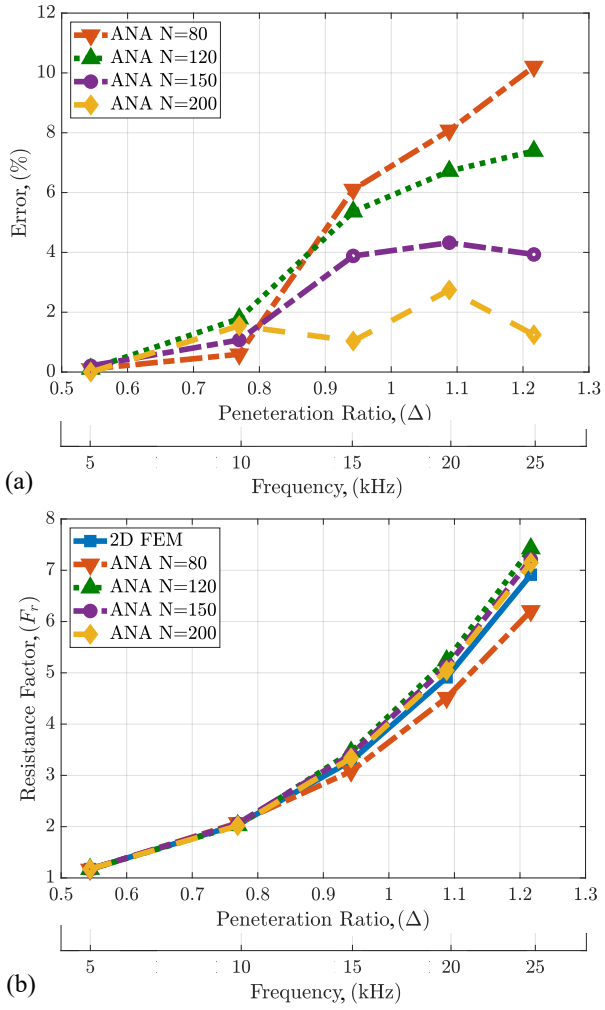

Fig. 5. Comparison of results in the frequency range of 5-25 kHz, calculated using FEM and semi-analytical method. (a) Resistance factor (b) Absolute deviation of R_F estimated using semi-analytical method compared to FEM.

stiffness matrix and source vector from COMSOL are exported to MATLAB. For the fairness of the comparison, both systems of equations derived from FEM and proposed approach, are solved using direct solver. A comparison of the simulation time is included in Table II. The solution with N=200 with 2.7% ε is slightly slower than FEM since the sparsity of system of linear equations in FEM is higher than the proposed method. However, the solution time for the semi-analytical method with N=150 is achieved with close to 2.5 times less processing time compared to FEM and with ε of 4.3%. Choosing a proper solver for the system of linear equations developed in the proposed method could provide the advantages of reduced dof. In addition, the reduced amount of dof enables a faster post processing. Finally, the mesh free approach can be added to the advantages of the proposed approach. The meshing time of the problem under study for this paper takes approximately half of the solving time which definitely contributes to computational burden in a design routine.

V. Conclusion

A mesh-free Fourier-based method is presented to model the AC winding loss in foil-wound MFTs. The proposed semi-analytical approach uses the Fourier-based representation of the position dependent conductivity in the foils and imposed current density in the window area of MFTs. The solution of the magnetic vector potential in the window area of MFT is used to calculate the AC loss and resistance factor of the MFT winding. Results obtained by the semi-analytical method for the frequency range of 5-25 kHz show that the size of the system of linear equations in the semi-analytical method is reduced by 2.5 times compared to FEM, and a good level of accuracy with maximum absolute error of 2.7% is achieved.

Acknowledgement

This paper is part of the project Advanced Solid State TRAnsformers (ASSTRA), which is an EU funded Marie Curie ITN project, grant number 765774.

References

[1] J. E. Huber, J. W. Kolar, "Applicability of Solid-State transformers in today's and future distribution grids," *IEEE Trans. Smart Grid,* vol. 10, no. 1, pp. 317-326, Jan. 2019.

[2] T. B. Gradinger, U. Drofenik, "Managing high currents in litz-wire-based medium-frequency transformers," in *Proc. European Conf. on Power Electron. and Appl. (EPE ECCE Europe)*, Riga, Latvia, 2018, pp. P.1-P.10.

[3] T. B. Gradinger, U. Drofenik, F. Grecki, "Enabling foil windings of medium-frequency transformers for high currents," in *Proc. European Conf. on Power Electron. and Appl. (EPE ECCE Europe)*, Lyon, France, 2020, pp. 1-10.

[4] K. Ramakrishnan, M. Curti, D. Zarko, G. Mastinu, J. J. H. Paulides, E. A. Lomonova, "Comparative analysis of various methods for modelling surface permanent magnet machines," *IET Eelec. Power Appl.*, vol. 10, no. 1, pp. 317-326, Jan. 2019.

[5] M. A. Bahmani, T. Thiringer, H. Ortega, "An Accurate pseudoempirical model of winding loss calculation in HF foil and round conductors in switch mode magnetics," *IEEE Trans. Power Electron.*, vol. 11, no. 4, pp. 540–547, Apr. 2017.

[6] P. L. Dowell, "Effects of eddy currents in transformer windings," *Proc. Inst. Electr. Eng.*, vol. 113, no. 8, p. 1387, Aug. 1966.

[7] F. Robert, P. Mathys, B. Velaerts, J. -P. Schauwers, "Two-dimensional analysis of the edge effect field and losses in high-frequency transformer foils," *IEEE Trans. Magn*, vol. 41, no. 8, pp. 2377-2383, Aug. 2005.

[8] D. Whitman and M. K. Kazimierczuk, "An analytical correction to dowell's equation for inductor and transformer winding losses using cylindrical coordinates," *IEEE Trans. Power Electron.*, vol. 34, no. 11, pp. 10425–10432, 2019.

[9] E. Bennett, S. C. Larson, "Effective resistance to alternating currents of multilayer windings," *A.I.E.E. Trans.*, vol. 59, no. 12, pp. 1010-1016, Dec. 1940.

[10] J. A. Ferreira, J. D. van Wyk, "A new method for the more accurate determination of conductor losses in power electronic converter magnetic components," *3rd Int. Conf. Power Electron.*, London, UK, 1988, pp. 184-187.

[11] J. A. Ferreira, "Improved Analytical Modeling of Conductive Losses in Magnetic Components," *IEEE Trans. Power Electron.*, vol. 9, no. 1, pp. 127–131, 1994.

[12] F. Robert, P. Mathys, "Ohmic losses calculation in SMPS transformers: numerical study of Dowell's approach accuracy," *IEEE Trans. Magn.*, vol. 34, no. 4 PART 1, pp. 1255–1257, 1998.

[13] C. H. H. M. Custers, J. W. Jansen, E. A. Lomonova, "2-D semi-analytical modeling of eddy currents in multiple non-connected conducting elements," *IEEE Trans. Magn.*, vol. 53, no. 11, pp. 1–6, 2017.

[14] B. L. J. Gysen, K. J. Meessen, J. J. H. Paulides, E. A. Lomonova, "General formulation of the electromagnetic field distribution in machines and devices using Fourier analysis," *IEEE Trans. Magn.*, vol. 46, no. 1, pp. 39–52, 2010.

[15] A. J. Jerri, "Lanczos-like σ-factors for reducing the Gibbs phenomenon in general orthogonal expansions and other representations," *JoCAAA*, vol. 2, no. 2, pp.111–127, 2000.